Simple models for quorum sensing: Nonlinear dynamical analysis

Wei-Yin Chiang,[1] Yue-Xian Li,[2] and Pik-Yin Lai[1,3,*]

[1]*Department of Physics, Graduate Institute of Biophysics and Center for Complex Systems, National Central University, Chungli, Taiwan 320, Republic of China*

[2]*Department of Mathematics and Department of Zoology, University of British Columbia, Vancouver, Canada V6T 1Z1*

[3]*Department of Physics, The Chinese University of Hong Kong, Shatin, Hong Kong, China*

(Received 22 June 2011; published 18 October 2011)

Quorum sensing refers to the change in the cooperative behavior of a collection of elements in response to the change in their population size or density. This behavior can be observed in chemical and biological systems. These elements or cells are coupled via chemicals in the surrounding environment. Here we focus on the change of dynamical behavior, in particular from quiescent to oscillatory, as the cell population changes. For instance, the silent behavior of the elements can become oscillatory as the system concentration or population increases. In this work, two simple models are constructed that can produce the essential representative properties in quorum sensing. The first is an excitable or oscillatory phase model, which is probably the simplest model one can construct to describe quorum sensing. Using the mean-field approximation, the parameter regime for quorum sensing behavior can be identified, and analytical results for the detailed dynamical properties, including the phase diagrams, are obtained and verified numerically. The second model consists of FitzHugh-Nagumo elements coupled to the signaling chemicals in the environment. Nonlinear dynamical analysis of this mean-field model exhibits rich dynamical behaviors, such as infinite period bifurcation, supercritical Hopf, fold bifurcation, and subcritical Hopf bifurcations as the population parameter changes for different coupling strengths. Analytical result is obtained for the Hopf bifurcation phase boundary. Furthermore, two elements coupled via the environment and their synchronization behavior for these two models are also investigated. For both models, it is found that the onset of oscillations is accompanied by the synchronized dynamics of the two elements. Possible applications and extension of these models are also discussed.

DOI: 10.1103/PhysRevE.84.041921 PACS number(s): 87.18.Hf, 05.45.Xt, 87.19.ln

I. INTRODUCTION

In biological systems such as D. discoideum (Dicty) [1–3], E. coli [4], and yeast [5], the cell population density is an important switch to turn "ON" and "OFF" the collective behavior of the cells. For Dicty, after a period of starvation, the cells will aggregate only when the chemical signals (cAMP) can propagate successfully. Cohen [2] proved analytically that, given the condition that a cell can only detect chemical signals above a certain concentration, the chemical signal cannot be propagated successfully if the cell population density is below a certain critical value. Similar results have been reported in experiments by Gingle [1]. Recently [6] it was observed that the motion of Dicty can undergo oscillation if the population density is high enough such that the extracellular cAMP concentration can induce intracellular cAMP oscillations. De Monte *et al.* [5] also showed that the glycolysis of yeast can only occur when the population density is high enough. The general phenomenon of switching to a different dynamical behavior collectively in response to the change in the population is referred to as quorum sensing (QS) [7]. Social insects such as ants [8] and honey bees [9] also employ QS to make decisions about new nest sites.

A similar QS-type phenomenon also appears in the chemical diffusion-reaction system [Belousov-Zhabotinsky (BZ) reaction]. Taylor *et al.* [10] showed that the dynamical behavior of the BZ reaction in cation-exchange beads in the solution also depends on the number density of the beads. Different dynamical behaviors can be observed at different exchange rates. The basic mechanism of quorum sensing can be understood as the following: The intracellular chemical signaling molecules produced by the cells diffuse to the extracellular environment and in turn affect other cells. There is always a net outward diffusion of chemicals secreted by the cell if the concentration of extracellular chemical signal and the cell population are both low. Because of this strong outward diffusion flux, there is no chance to sustain intracellular chemical oscillation. However, chemical oscillations can be sustained easily for sufficiently high cell population density. This is because even only a small amount of chemical signal molecules diffuse from each cell can increase the total extracellular chemical signal concentration substantially, which in turn interact with the cells and sustain chemical oscillations. The general model in Ref. [5] showed that such population density dependent behavior can occur in any collection of oscillators coupled to an extracellular medium by diffusion, provided that this diffusion is fast compared to the time scales of the dynamics of the amplitude and phase. However, it has been shown in Ref. [10] that different dynamical behaviors results when different exchange rates were applied. This exchange rate can be interpreted as the coupling strength between the concentrations of the signaling molecules inside and outside of the cell.

In this work, we aim at constructing the simplest possible model to describe the essential features of quorum sensing. The simplest model to describe oscillations is by using a phase model. A sufficiently simple model allows one to perform detailed analytic studies to gain insights for the

*pylai@phy.ncu.edu.tw

dynamical mechanisms in quorum sensing behavior. We further modify the well-known FitzHugh-Nagumo model with a population density parameter to investigate the transition of the dynamics while increasing the population density under different conditions (such as coupling strengths and degradation rates). The nonlinear dynamics of these models are analyzed and different interesting dynamical behaviors with different coupling strengths are obtained.

II. PHASE MODEL

Quorum sensing can be described by simple phase models. In phase models, the dynamics is described by the phase variable ϕ, and quiescent and oscillatory states are represented by the asymptotic conditions $\dot{\phi} = 0$ and $\dot{\phi} > 0$, respectively. Here we adopt the Kuramoto-type phase model [11] to describe the dynamics of a cell and couple it with the extracellular solution.

In general the chemical signal of a cell can be oscillatory or excitable when it is isolated (not coupled to the solution), but when it is immersed in a large volume of buffered solution, it is quiescent due to the severe diffusion of the chemical signal molecules from the interior of the cell to the extracellular solution. Increasing the cell number in the solution will retard this diffusion and can mark the onset of chemical oscillation of the cell as well as in the solution. The phases of the cell and the solution are denoted, respectively, by ϕ and Φ. Quorum sensing is modeled by the modified Kuramoto model as

$$\dot{\phi}_i = 1 - b_i \sin\phi_i + g \sin(\Phi - \phi_i), \tag{1}$$

$$\dot{\Phi} = \alpha \sum_N g \sin(\phi_i - \Phi) - J(\Phi - \Phi_0). \tag{2}$$

The intrinsic dynamics of an isolated cell is governed by the parameter $b > 0$ ($b < 1$: oscillatory; $b > 1$: excitable; and separated by an infinite-period bifurcation). g is the coupling strength and α is the conversion parameter, related to the volume fraction of a cell in the solution. The first term in Eq. (2) represents the contribution to the phase of the solution from a single cell. The dynamics of the phase in solution is attributed from all the cells in the solution. $\Phi_0 > 0$ is the constant resting state value of Φ of the stand-alone solution, and J is the corresponding relaxation rate of Φ to Φ_0. Φ_0 can be thought of as a quantity that originates from the concentration difference between the interior of the cell and the extracellular solution that the living cell would try to maintain due to homeostasis.

To allow further analytic studies, here we consider the mean-field approximation so that all the ϕ_i are replaced by the mean phase ϕ; such an approximation will be exact if all the cells are synchronized in phase. Under the mean-field approximation, Eqs. (1) and (2) can be reduced to

$$\dot{\phi} = 1 - b \sin\phi + g \sin(\Phi - \phi), \tag{3}$$

$$\dot{\Phi} = \gamma g \sin(\phi - \Phi) - J(\Phi - \Phi_0). \tag{4}$$

In the following subsections, we present detailed nonlinear dynamics analysis of the mean-field phase model given by Eqs. (3) and (4) by first characterizing the parameter regimes in which QS is relevant. Then due to the simplicity of the mean-field system, the equation for the fixed points can be derived analytically and determined. By examining in detail the nullclines and phase flow in the phase portrait (given in detail in the Appendix), the stability of the fixed points, and hence whether the system is quiescent or oscillatory, can be determined precisely. The full oscillatory or quiescent phase diagrams are then obtained with the equations governing the phase boundary derived explicitly. Finally, we consider the case of relaxing the mean-field assumption by considering two cells in the medium and show that the onset of oscillation is accompanied by the synchronization of the two cells. A similar analysis procedure is employed in the next section for the FitzHugh-Nagumo type model for QS.

A. $b - g$ parameter space

It is instructive to rewrite Eq. (3) as

$$\dot{\phi} = 1 - R \sin(\phi - \psi), \tag{5}$$

where

$$R^2 = b^2 + 2bg\cos\Phi + g^2, \tag{6}$$

$$\psi = \tan^{-1}\left(\frac{g\sin\Phi}{b + g\cos\Phi}\right). \tag{7}$$

R is a function of Φ and hence its value is time dependent. Note that $R \leqslant b + g$ and $R \geqslant |b - g|$. If $R < 1$ holds in the long time limit, $\dot{\phi}$ is always positive and hence the system is oscillatory, e.g., when $b + g < 1$. Similarly, if $R > 1$ always holds, the system will remain quiescent, e.g., when $|b - g| < 1$. Hence from Eq. (6), one can see that Φ can drive the system to oscillate when it is coupled to ϕ. From the above argument, it is easy to show that the system always remains quiescent if $|b - g| > 1$, and always oscillates if $b + g < 1$. But it should be cautioned that an asymptotically oscillatory system can have R vary periodically covering both the >1 and <1 regimes.

Next we further derive the condition for a single cell to remain quiescent when it is immersed in a large volume of extracellular solution. This is the situation that we are interested in modeling the quorum sensing behavior. In this infinite dilution limit, $\gamma \sim 0$, Eq. (4) gives $\Phi \sim \Phi_0$ for $t \to \infty$ and ψ takes a constant value. Therefore the criteria for this single immersed cell to be quiescent is $b^2 + 2bg\cos\Phi_0 + g^2 > 1$. For a given value of Φ_0, we shall choose values of b and g to satisfy the above condition and refer to this regime as the quorum sensing or QS regime. The parameter regimes of interests is summarized in the b-g plane shown in Fig. 1. In some scenarios, increasing γ will increase Φ and could elicit oscillation of ϕ. The cause of this oscillatory behavior with increasing γ can be inferred as "quorum sensing." From Eq. (6), oscillatory behavior is favored when R is small, i.e., $\cos\Phi < 0$ or $\frac{\pi}{2} < \Phi < 3\pi/2$.

In this paper, quorum sensing refers to the original quiescent state for low values of γ, which becomes oscillatory as γ is increased. In general, the present phase model can produce quorum sensing for arbitrary values of Φ_0. In this paper since we are mostly studying cells with $b \sim 1$, $\Phi_0 = 2$ is used in all the numerical results.

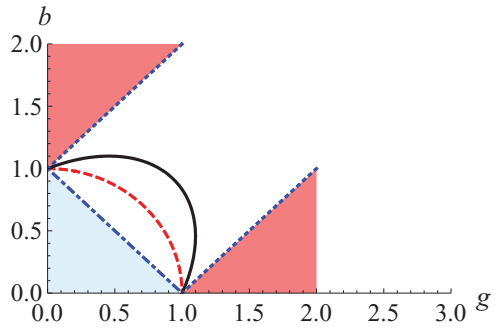

FIG. 1. (Color online) Parameter space in the b-g plane. The boundary lines and curves are given by $b^2 + 2bg\cos\Phi_0 + g^2 = 1$ for different values of Φ_0. Dotted lines: $|b - g| = 1$ ($\Phi_0 = \pi$). Dot-dashed line: $b + g = 1$ ($\Phi_0 = 0$). Dashed curve: $\Phi_0 = \frac{\pi}{2}$. Solid curve: $\Phi_0 = 2$. The blue (shaded triangular region near the origin) and pink (the other two shaded regions) areas mark the parameter regimes in which the system is always oscillatory or quiescent, respectively. The values of b and g are to be chosen in the region bound by the black solid curve and dotted lines to ensure that the cell is quiescent in the infinite dilution limit, and is referred to as the QS regime in this paper.

B. Fixed points and phase space

In the two-dimensional dynamical system described by Eqs. (3) and (4), oscillations occur when the stable fixed point disappears. The fixed points can be solved from the intersections of the nullclines. The nullclines $\dot\phi = \dot\Phi = 0$ are given by the equations

$$g\sin(\phi - \Phi) = 1 - b\sin\phi \quad \text{or} \quad R\sin(\phi - \psi) = 1, \tag{8}$$

$$\Phi = \Phi_0 + \Gamma g\sin(\phi - \Phi), \tag{9}$$

where $\Gamma \equiv \gamma/J$. The $\dot\phi = 0$ nullcline can be solved explicitly to give $\phi(\Phi) = \psi + \sin^{-1}\frac{1}{R}$. Detailed analysis of the properties of the nullcines and corresponding phase space flow portraits are presented in the Appendix. As can be seen in Fig. 12, the fixed points always emerge in pairs except at the critical parameter values. From the analysis of the flow fields in the phase portrait and the fixed points, it is clear that there is at least one stable fixed point (hence the system is quiescent) whenever more than one fixed point exists.

It is easy to see from Eqs. (3) and (4) that the fixed point (ϕ^*, Φ^*) is given by

$$F(\phi^*) \equiv 1 - b\sin\phi^* + g\sin[\Gamma(1 - b\sin\phi^*) - \phi^* + \Phi_0] = 0, \tag{10}$$

$$\Phi^* = \Phi_0 + \Gamma(1 - b\sin\phi^*). \tag{11}$$

ϕ^* can be found from the roots of Eq. (10) for different Γ and g. The fixed points and their stability are shown in Fig. 2 for different values of b and g. For a stable fixed point, the trace and determinant of the Jacobian matrix at the fixed point must be negative and positive, respectively.

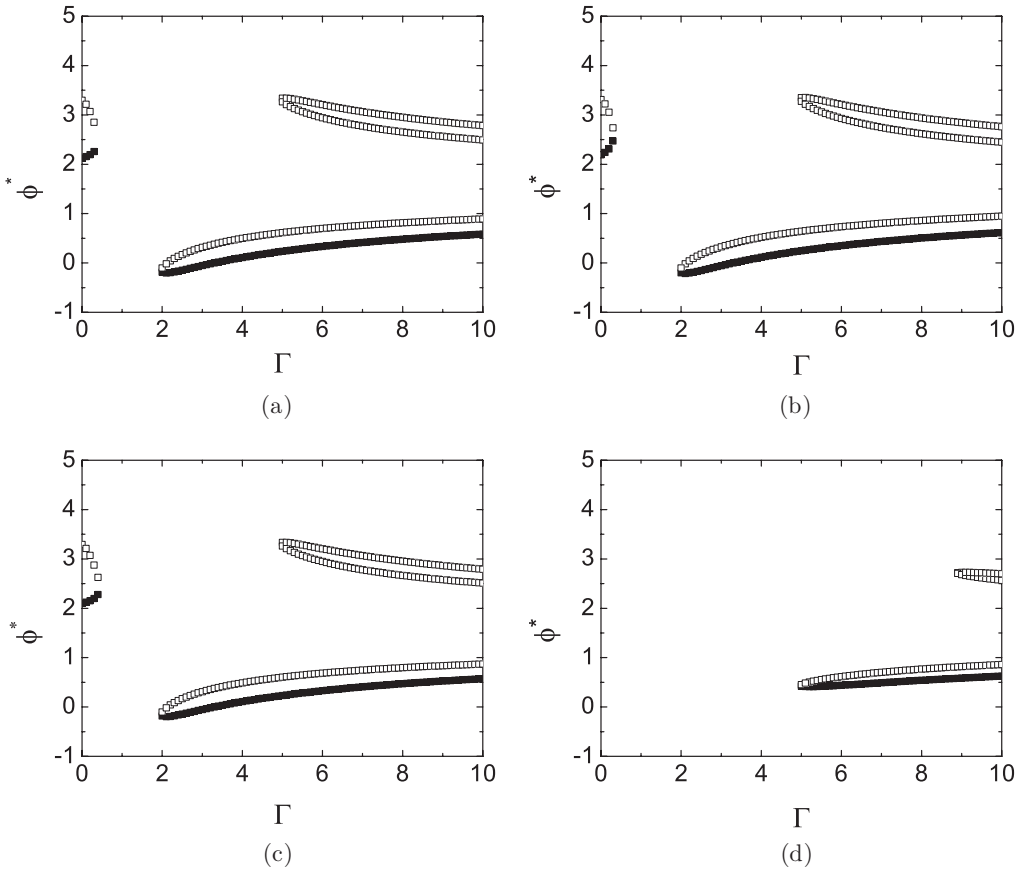

FIG. 2. Fixed points ϕ^*, and the associated stability obtained by the method mentioned in text for (a) $b = 1$, $g = 1.2$, (b) $b = 0.95$, $g = 1.2$ (c) $b = 1.02$, $g = 1.2$, and (d) $b = 1$, $g = 0.6$. Filled symbols: stable. Open symbols: unstable.

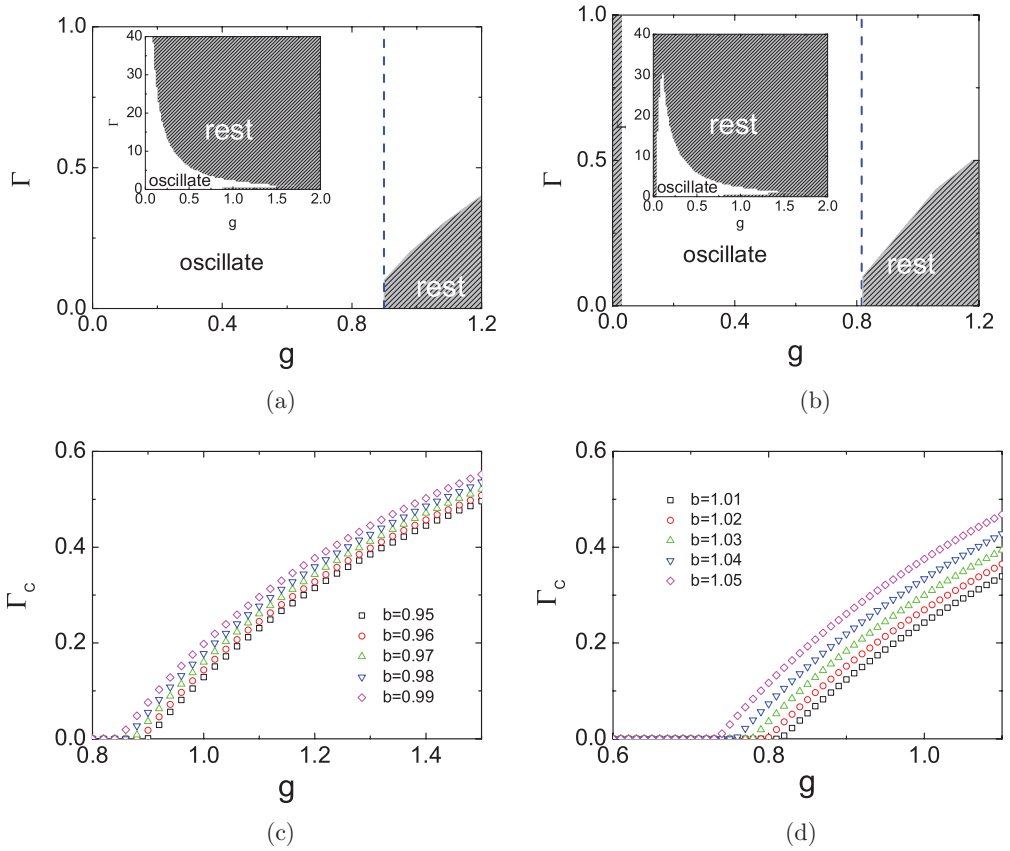

FIG. 3. (Color online) Phase diagrams from the phase model for quorum sensing. (a) Phase diagram for intrinsically oscillatory cells, showing different dynamics for different Γ and g ($b = 0.95$). The shadow area is the quiescent region bounded by the phase boundary Γ_c. The vertical dashed line marks the region of interest ($b^2 + 2bg\cos\Phi_0 + g^2 > 1$, right-hand side of the dashed line) in modeling quorum sensing. The inset shows regions for larger Γ in which Γ_u can be seen; it covers regions that are beyond biological interest for the present study and are shown here just for completeness. (b) Phase diagram for intrinsically excitable cells ($b = 1.01$). Dashed line and the inset have the same meaning as in (a). (c) Critical Γ_c vs the coupling strength corresponds to the phase diagram in (a) for various values of b. (d) Critical Γ_c vs the coupling strength corresponds to the phase diagram in (b) for various values of b.

Since fixed points always emerge in pairs (except at the critical parameter values) and there is at least one stable fixed point whenever more than one fixed point exists, the problem of determining whether the system is quiescent or oscillatory reduces to the existence or absence of real roots of $F(\phi^*)$ in Eq. (10).

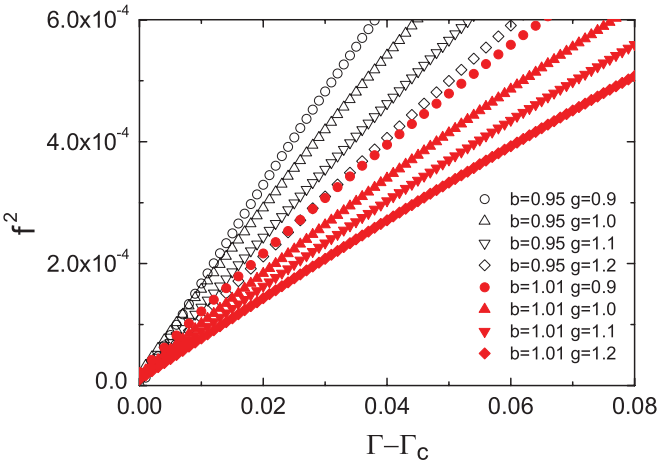

FIG. 4. (Color online) Square of the oscillation frequency as a function of $\Gamma - \Gamma_c$ for the quorum sensing transition regime with $b = 0.95$ and $b = 1.01$ for different values of g ($J = 1$). The oscillation frequency varies with the square root of $\Gamma - \Gamma_c$ implying an infinite-period bifurcation.

C. Phase diagrams

The phase diagram for intrinsically oscillatory cells ($b < 1$) is depicted in Fig. 3(a), there is an oscillatory region for smaller values of g and Γ covering the origin and the whole Γ axis. For sufficiently large g, the system becomes quiescent. The QS regime ($b^2 + 2bg\cos\Phi_0 + g^2 > 1$) as discussed in Fig. 1 is shown by the right-hand side of the dashed line. In the QS regime, the system is quiescent for low values of Γ, and as Γ increases above some critical value Γ_c, the system becomes oscillatory. A new stable fixed point appears when Γ is further increased beyond another threshold Γ_u and oscillation stops again. The phase diagram for intrinsically excitable cells ($b \gtrsim 1$) is depicted in Fig. 3(b); there is a finite domain for oscillation—note that now there is a thin quiescent strip near $g \gtrsim 0$, which corresponds to the always quiescent regime $g < b - 1$ as discussed in Fig. 1. Oscillations only occur for intermediate values of coupling strength. This is because the

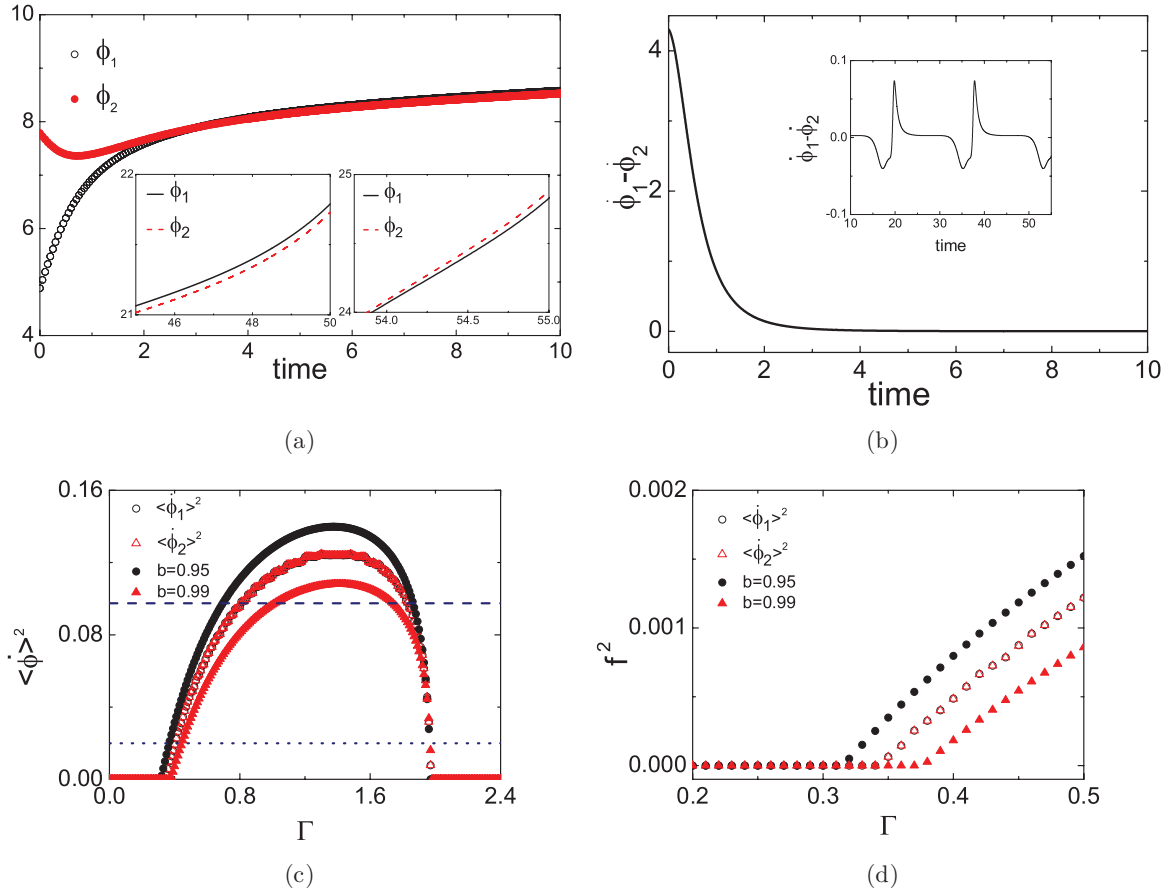

FIG. 5. (Color online) Simulation result for two heterogenous cells showing synchronization as collective oscillations emerges. $J = 1$, $g = 1.2$, $b_1 = 0.95$, $b_2 = 0.99$. Note that the mean angular frequencies of the two cells under isolated condition are 0.312 25 and 0.141 07, respectively. (a) Time series of $\phi_1(t)$ and $\phi_2(t)$ with different initial conditions; $\Gamma = 0.6$. The insets show the blowup scale so that the small phase differences can be seen. Note that in some period ϕ_1 leads ϕ_2 (left inset), but it is reversed at later times (right inset). (b) Difference in the instantaneous angular velocities of two oscillatory cells in (a). The inset is a magnified scale showing that the instantaneous angular velocity difference oscillates about zero, and the two cells have no phase-locked synchronization. (c) Average asymptotic angular velocities of the two cells as a function of Γ. The angular frequencies for each of the single cells in the medium with the same $g = 1.2$ are also shown for comparison. The horizontal straight lines indicate the angular frequencies ($\sqrt{1-b^2}$) for each of the cells under isolated conditions (not coupled to the medium). (d) The square of the average asymptotic angular frequencies plotted as a function of Γ near the critical regime showing the saddle-node (infinite-period) bifurcation behavior.

driving force from coupling in the weak coupling regime may be too weak to elicit the oscillation, but on the other hand oscillation will also disappear if the coupling is too strong. In the QS regime of Fig. 3(b), an oscillatory window also exists for $\Gamma_c < \Gamma < \Gamma_u$. In general, there is a lower and upper critical value for Γ in the QS regime for the phase model, i.e., some regime of cell population density in which oscillations occur. However, we emphasize that we are interested mainly in the transition from quiescence to oscillations as the number of cells increases from a system with low cell volume fraction.

The critical Γ_c (and also Γ_u) can be obtained by solving the fixed point equation $F(\phi^*)$ in Eq. (10) together with $F'(\phi^*) = 0$:

$$b\cos\phi^* = -g(1 + b\Gamma_c\cos\phi^*)\cos[\phi^* - \Phi_0 - \Gamma_c(1 - b\sin\phi^*)]. \quad (12)$$

The critical Γ_c vs g for different values of b is shown in Figs. 3(c) and 3(d). The dynamics of the cells changes from quiescent to oscillation when Γ exceeds Γ_c. In general, Γ_c increases with both g and b.

The oscillation frequency can be obtained from the numerical solution of the ordinary differential equations (ODEs) and it is found that the frequency decreases for decreasing γ as shown in Fig. 4 . For the quorum sensing transition from quiescence to oscillation across Γ_c, the oscillation frequency varies with the square root of $\Gamma - \Gamma_c$ indicating an infinite-period bifurcation.

D. Synchronization

In the above analysis, we adopted the mean-field approximation, which is based on the implicit assumption that each cell will synchronize when they start to oscillate. Here we shall show explicitly in the simple case of two cells that the synchronization is accompanied by the emergence of oscillations. Synchronization [12] is one of the most prominent signatures of collective behavior in a cell population, and quorum sensing is believed to be the major communication

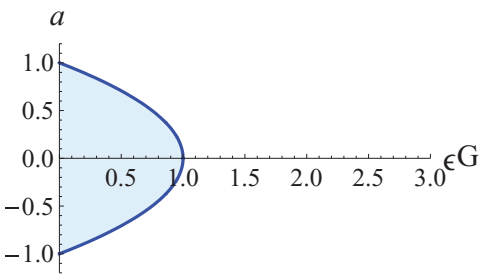

FIG. 6. (Color online) Parameter space in the a-G plane. QS regime is the unshaded area.

mechanism that leads to this cooperative phenomenon. In order to make a fair comparison for the sensitivity of quorum sensing for systems with different number of cells, instead using the single cell parameter α, one can define $\Gamma = N\alpha/J$ similar to the mean-field approximation case in previous sections. Consider for simplicity only two heterogeneous cells described by Eqs. (1) and (2) with $b_1 \neq b_2$. It is easy to show that constant phase difference synchronization is not possible when b_1 is not equal to b_2. Thus we shall consider the general phase-locked synchronization in which the phase difference obeys some relationship and is bounded. A convenient measure to show this type of synchronization in the present study is to compare their average oscillation frequencies. This operational measure is valid here since we know the two oscillators are coupled via a shared chemical signal. The two elements are synchronized if they have the same average oscillation frequencies, i.e., $\langle\dot{\phi}_1\rangle = \langle\dot{\phi}_2\rangle$ (where $\langle\cdots\rangle$ denotes the long time average after the system passed the transient state). Direct simulation of the systems shows that for small values of Γ, both cells are quiescent, but when Γ is greater than some critical value, the two cells start to be oscillatory and very soon become synchronized with a small phase difference as shown in Fig. 5(a) . Furthermore, the phase difference oscillates between positive and negative values as illustrated in the insets. The instantaneous angular velocities shown in Fig. 5(b) confirm that the two elements synchronized very rapidly with the angular velocity difference oscillate about zero (see inset) and the two elements synchronized with the same mean angular velocity. Note that the mean angular frequency of an isolated intrinsically oscillatory cell is $\sqrt{1-b^2}$. Figure 5(c) shows the asymptotic mean angular speeds of the two oscillatory cells as a function of Γ, indicating a regime $\Gamma_c < \Gamma < \Gamma_u$ in which synchronized oscillations occur, similar to the results obtained under the mean-field analysis. Furthermore, the onset of oscillation also occurs via an infinite-period bifurcation as verified in Fig. 5(d), which shows the oscillation frequency $\propto \sqrt{\Gamma - \Gamma_c}$.

III. FITZHUGH-NAGUMO MODEL

Unlike phase models, oscillations in the FitzHugh-Nagumo (FHN) model [13] dynamical system is characterized by the emergence of a stable limit cycle in phase space. To model quorum sensing, consider the simple FHN with fast variable coupled to the extracellular environment variable Z; the dynamics is given by

$$\frac{dx}{dt} = \frac{1}{\epsilon}\left(x - \frac{x^3}{3} - y\right) + G(Z - x), \tag{13}$$

$$\frac{dy}{dt} = x + a. \tag{14}$$

The FHN element can be either excitable ($|a| > 1$) or oscillatory ($|a| < 1$). To describe chemical reactions, x can be interpreted as the deviation of signal molecule concentration inside the cell from some reference concentration (denoted by X_M). These signal molecules can exchange with the environment (denoted by Z, the deviation of extracellular signal molecule concentration from X_M) with a coupling G. The dynamics of signaling chemical concentration in the environment can be described by

$$\frac{dZ}{dt} = -J(Z + X_M) + \alpha G(x - Z), \tag{15}$$

where α is the volume fraction of a single cell to that of the environment, and J is the degradation rate. For a population

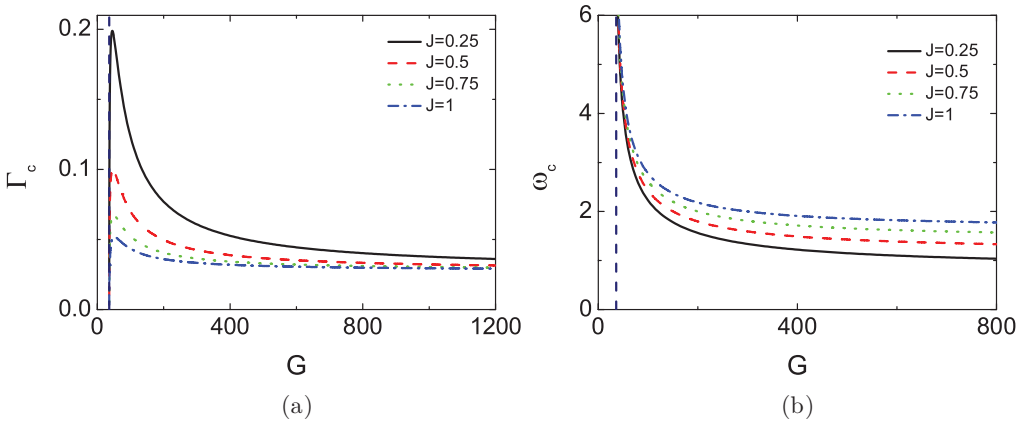

FIG. 7. (Color online) FitzHugh-Nagumo quorum sensing model, $a = 0.8$, $\epsilon = 0.01$. (a) Critical Γ_c above which the stable node bifurcates to limit cycle oscillation via Hopf bifurcation, as a function of coupling strengths G for different degradation rates. The bifurcation curve is calculated from Eq. (19). (b) Emergent frequency at the bifurcation point as a function of G for various values of J, calculated from Eq. (20). The vertical dashed line marked $G^* = 36$: Hopf bifurcation occurs for $G > G^*$.

of the FHN elements in the medium, the dynamics of Z can be rewritten as

$$\frac{dZ}{dt} = -J(Z + X_M) + \alpha G \sum_i (x_i - Z). \tag{16}$$

If we only consider the situation that all of the cells oscillate and synchronize in phase, mean-field approximation gives

$$\frac{dZ}{dt} = -J(Z + X_M) + \gamma G(x - Z), \tag{17}$$

where γ is the ratio of total cell volume to the volume of solution in the environment. X_M should be sufficiently positive so that both $x + X_M$ (the intracellular chemical concentration) and $Z + X_M$ are always non-negative. $X_M = 2$ is taken in this paper, which satisfies the above requirement. Similar to the previous section, the dynamical behavior given by Eqs. (13), (14), and (17) is analyzed for different coupling strengths G, as γ is varied.

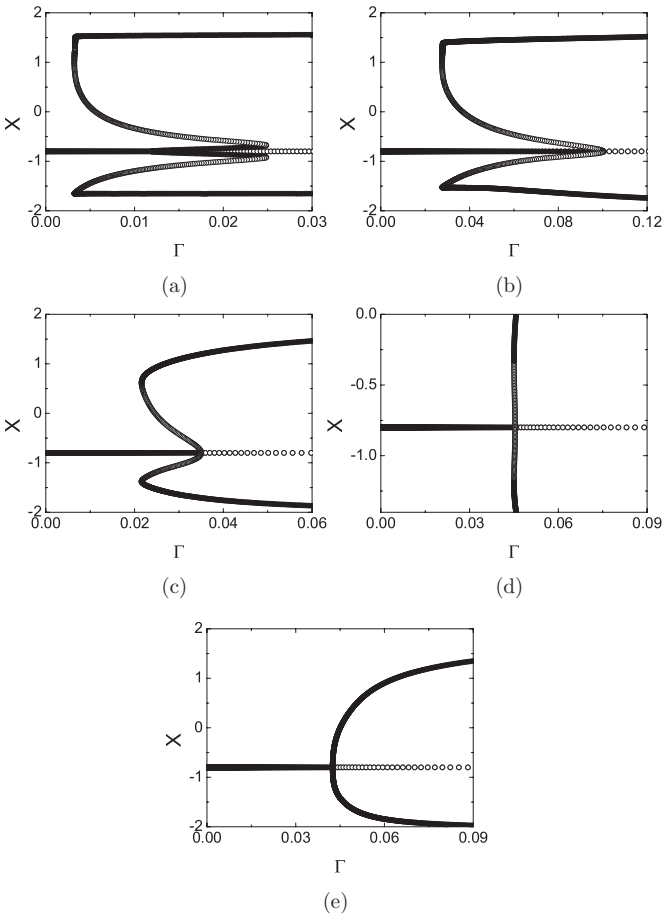

FIG. 8. Bifurcation diagrams for the FHN quorum sensing model with $a = 0.8, J = 0.5, X_M = 2$, and $G^* = 36$. (a) $G = 36.06$: fold-cycle and supercritical Hopf bifurcation. Note the coexistence of large (outer) and small (inner) amplitude oscillations. (b) $G = 46.55$: fold-cycle and subcritical Hopf bifurcation. The small amplitude stable limit cycle in (a) just annihilated with its surrounding unstable limit cycle. (c) $G = 100$: fold-cycle and subcritical Hopf bifurcation. (d) $G = 250$: fold-cycle and subcritical Hopf bifurcation occur in a very narrow regime of Γ, and the dynamics of the system is about to change to (e). (e) $G = 300$: supercritical Hopf bifurcation. In the very strong coupling regime, the unstable limit cycle in (d) shrinks to an unstable fixed point resulting in a supercritical bifurcation.

For quorum sensing, one usually encounters the situation that there is no spontaneous oscillation when a single cell is coupled with the solution (corresponding to infinite dilution of cell population density, $\gamma = 0$ case) [5], but oscillation emerges as cell density increases. For the model described by Eqs. (14) and (17), it can be shown later that for $|a| > 1$ there is no bifurcation to oscillatory state for any positive values of γ, therefore we here consider only the case of $|a| < 1$. For $\gamma = 0$ and from Eq. (13), the condition for a stable fixed point leads to the criteria $G > G^* \equiv \frac{1-a^2}{\epsilon}$. A FHN element immersed in the solution will be oscillatory (quiescent) if $G < G^*$ ($G > G^*$). Figure 6 show the parameter regime corresponding to the QS regime.

A. Hopf bifurcation

The fixed point of the system (13), (14), and (17) is easily calculated to be

$$\begin{aligned} x_f &= -a, \\ y_f &= -a + \frac{a^3}{3} + \epsilon G(Z_f + a), \\ Z_f &= -\frac{\Gamma G a + X_M}{\Gamma G + 1}, \end{aligned}$$

where $\Gamma \equiv \frac{\gamma}{J}$ as in the phase model. In general, the fixed point becomes more stable as coupling strength is increased. If $\Gamma G \gg 1$ then $Z_f \approx -a$. If $\Gamma G \ll 1$ then $Z_f \approx -X_M$. The Jacobian at the fixed point and the corresponding characteristic equation for the eigenvalues at the fixed point can be easily computed to give

$$\begin{aligned} &\lambda^3 + A\lambda^2 + B\lambda + C = 0, \quad \text{where} \\ &A \equiv J(1 + \Gamma G) + G - G^*, \\ &B \equiv \frac{1}{\epsilon} + J[G - G^*(1 + \Gamma G)], \\ &C \equiv \frac{J}{\epsilon}(1 + \Gamma G). \end{aligned} \tag{18}$$

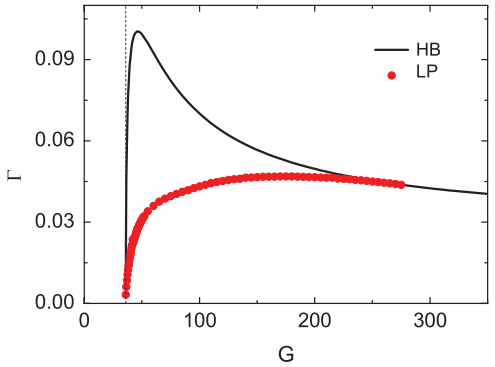

FIG. 9. (Color online) Phase diagram for the FHN quorum sensing model. Upper curve is the Hopf bifurcation (HB) boundary from Eq. (19). Lower symbol curve denotes the limit points (LP) obtained numerically from XPPAUT, where global bifurcations occur. Vertical dashed line marks the value of G^*.

Note that since $C > 0$ always holds, there is always a real and negative root for the eigenvalue Furthermore, if all the three eigenvalues are real, the other two roots must be of the same sign. Therefore it will be impossible for the stable node to lose its stability to become a saddle node since it would occur when the other two roots are zero, which is not allowed since $C > 0$. Hence there is one negative real eigenvalue and two complex eigenvalues (with nonzero imaginary parts), and the stable node loses its stability via Hopf bifurcation. The Hopf bifurcation condition or the phase boundary for the stability of the fixed point can be calculated from the condition that the real parts of the complex eigenvalues become zero. Simple calculation leads to the Hopf bifurcation condition of $AB = C$, i.e., the critical Γ_c satisfies the following algebraic equation:

$$\{1 + \epsilon J[G - G^*(1 + \Gamma_c G)]\}[J(1 + \Gamma_c G) + G - G^*] = J(1 + \Gamma_c G) \tag{19}$$

and Γ_c can be obtained as a function of G and other parameters. The emergent oscillation frequency at the bifurcation point as a function of G can also be calculated to give

$$\omega_c = \sqrt{B(\Gamma_c)} = \sqrt{\frac{1}{\epsilon} + J[G - G^*(1 + \Gamma_c G)]}. \tag{20}$$

Note that at $G = G^*$, $\Gamma_c = 0$, and $\omega_c = \sqrt{1/\epsilon}$. Furthermore, it is easy to see from Eq. (19) that there is no positive solution for Γ_c for $G^* < 0$ ($|a| > 1$), and hence we only consider the case of $|a| < 1$. The Hopf bifurcation phase boundary calculated from Eq. (19) is shown in Fig. 7. Γ_c shows a peak as a function of G, and decreases with the degradation rate J. The magnitude of the oscillation frequency is characterized by the emergent angular frequency ω_c, whose variation with G for various J is shown in Fig. 7. ω_c decreases monotonically with G and J.

B. Global bifurcation

However, the above analysis near the fixed point can only detect local bifurcations, for possible global bifurcation we employed XPPAUT [14] for numerical detection. Figure 8 shows that global bifurcation to oscillations indeed occurs in some parameter regimes. The bifurcation structure is surprisingly complicated for this model. It turns more complicated as the value of G decreases from a large value, say 300, when a simple supercritical Hopf bifurcation occurs [see Fig. 8(e)]. As G decreases, the Hopf bifurcation first becomes subcritical while the oscillations turn more relaxation type [see Figs. 8(c) and 8(d)]. At a G value slightly larger but close to G^* [see Figs. 8(a) and 8(b)], the Hopf bifurcation turns supercritical again giving rise to a branch of small amplitude periodic

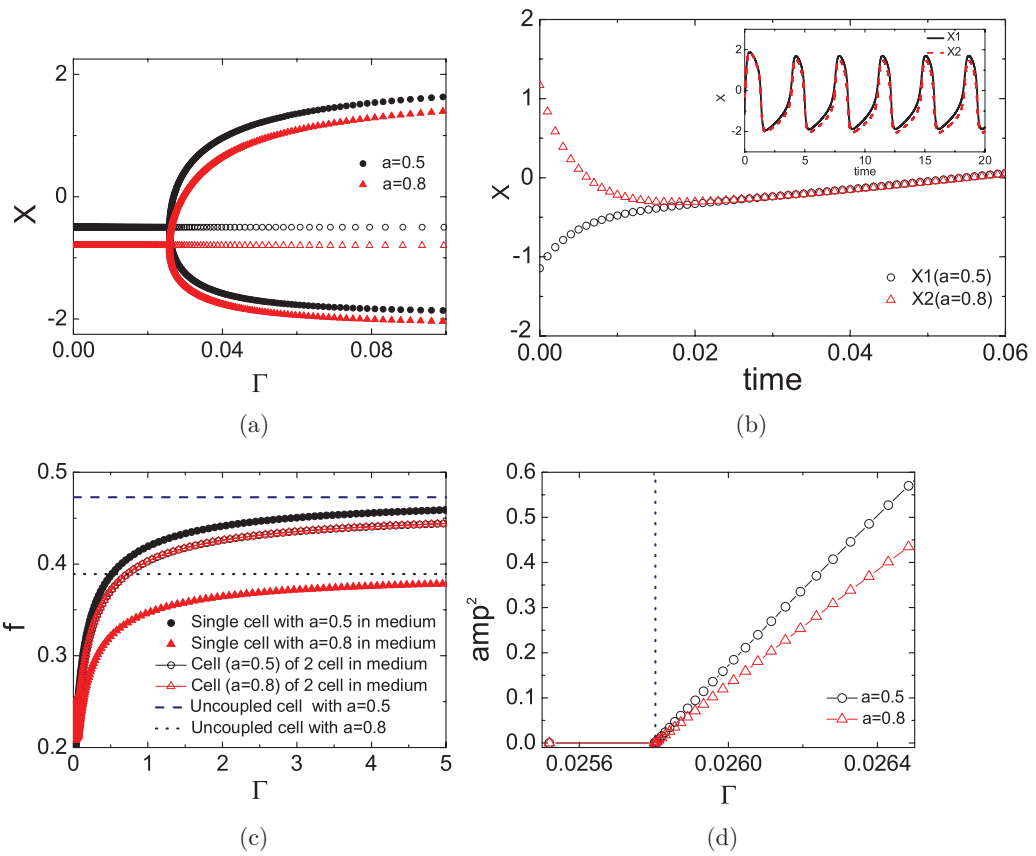

FIG. 10. (Color online) Simulation result for two heterogenous FHN cells showing synchronization as collective oscillations emerge via Hopf bifurcation. $a_1 = 0.5$, $a_2 = 0.8$, $J = 0.5$, and $G = 300$. (a) The coupled system undergoes a Hopf bifurcation at some critical Γ_c. (b) Time series of the two cells showing in-phase synchronized oscillations. $\Gamma = 0.04$. (c) Oscillation frequencies of the two cells showing synchronized oscillations as oscillations emerged. (d) The square of the oscillation amplitudes of the two cells as a function of γ, verifying a supercritical Hopf bifurcation. The vertical dashed line marks $\Gamma = \Gamma_c$.

solutions that coexist with the branch of large amplitude ones. This occurs at a cusp bifurcation for some critical value of Γ.

The phase diagram summarizing the quiescent or oscillatory behavior is shown in Fig. 9. For $G > G^*$, the region below the boundary of the limit point curve (low Γ) is always quiescent whereas the region above the Hopf bifurcation (HB) curve (high Γ) is always oscillatory. Note that the limit point (LP) curve ends at some large coupling value. The region bounded by the HB and LP curves is the coexistence in which quiescent or oscillatory dynamics are both possible depending on the initial conditions of the system.

C. Synchronization

In the quorum sensing model, the cells in the medium are coupled indirectly with each other via their coupling with the environment. This indirect intercell coupling can lead to synchronized dynamics and affect the quorum sensing sensitivity. In this case, the dynamics is governed by Eq. (16). Here we consider the simple case of two FHN cells coupled with the environment and examine the synchronization behavior as the cells become oscillatory. Again similar to the case of the phase model in the previous section, one defines $\Gamma = N\alpha/J$ in order to compare a system with different number of cells. For simplicity we take $G = 300$ so that a single cell will undergo Hopf bifurcation and become oscillatory (see Fig. 9). For low values of Γ, both cells are quiescent and become oscillatory when $\Gamma > \Gamma_c$ [see Fig. 10(a)] . Furthermore, both cells become synchronized as oscillations emerge [see Fig. 10(b)]. The two cells appear to be in-phase synchronized. The oscillation frequencies as a function of Γ for each single cell in the medium and the synchronized frequency when both are in the medium are shown in Fig. 10(c). The cells oscillate faster with Γ, and furthermore when both cells are in the medium, they synchronize and oscillate with a "compromised frequency." Notice that the Γ_c for each single FHN element in the medium are 0.018 759 8 ($a_1 = 0.5$) and 0.042 493 ($a_2 = 0.8$), respectively. When both of them are placed in the environment and coupled via the medium, oscillations emerge at an in-between $\Gamma_c \simeq 0.0258$ [see Fig. 10(d)]. Figure 10(d) shows that the oscillation amplitude $\propto \sqrt{\Gamma - \Gamma_c}$ verifying a supercritical Hopf bifurcation.

For completeness, we also examine the onset of oscillations and synchronization of two cells via global bifurcation with $G = 100$. Figure 11(a) shows that as Γ increases, fold or subcritical bifurcation occurs for the two cells simultaneously. The onset of oscillations of the two cells is accompanied by in-phase synchronization. Figure 11(b) shows the oscillation

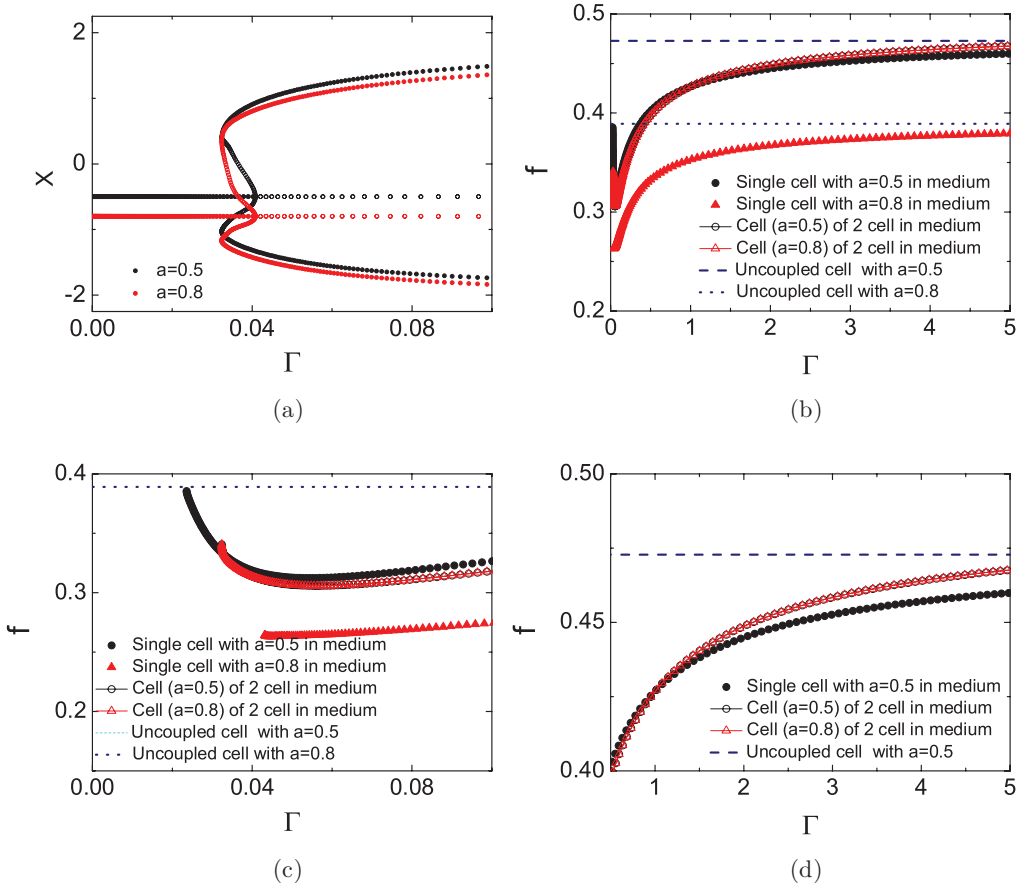

FIG. 11. (Color online) Simulation result for two heterogenous FHN cells showing synchronization as collective oscillations emerge via global bifurcation. $a_1 = 0.5$, $a_2 = 0.8$, $J = 0.5$, and $G = 100$. (a) The coupled system undergoes a global bifurcation at some critical Γ_c. (b) Oscillation frequencies of the two cells showing synchronized oscillations as oscillations emerge. (c) Magnification of (b) in the small Γ regime showing the nonmonotonic behavior in oscillation frequencies as a function of Γ. (d) Magnification of (b) in the larger Γ regime showing the frequency enhancement effect.

frequencies of the cells as compared with the oscillation of each single cell in the medium. The frequencies of the two cells coincide as oscillation emerges for $\Gamma > \Gamma_c$. Figure 11(c) is a blowup for small Γ showing the nonmonotonic variation of the synchronized frequencies with Γ. Note that for small values of Γ, the two cells are synchronized with a compromised frequency lying between the frequencies of each single cell in the medium. However, for larger values of Γ [see Fig. 11(d)], the two cells oscillate with a faster synchronized frequency, exhibiting the "frequency enhancement" effect [15].

IV. DISCUSSION

Two simple models aimed at describing some basic features of the switch in dynamical behavior in response to the change in population as observed in quorum sensing scenarios are proposed. The dynamics is investigated both by analytic means and also by numerical integrations, and the change in dynamics is understood in terms of bifurcations using nonlinear dynamic analysis. Mean-field theory is employed in most of our analysis. There are two major assumptions in this approximation: (i) all cells are assumed to oscillate in phase, and (ii) diffusion of the signaling chemicals in solution is so fast that one can regard its concentration to be uniform. The first assumption is justified by our study of two cells immersed in solution and practically in-phase synchronized oscillations are observed. The second assumption of the spatially uniform concentration can be realized experimentally by external stirring. However, for unstirred systems, diffusion of the signaling chemicals in solution would play an important role in governing the quorum sensing behavior [16]. Our model can be easily generalized to include the diffusion dynamics together with the spatial temporal description of the cells and signaling molecule concentration. The general question of the quorum sensing onset and phase-locked synchronized oscillations of an ensemble of elements indirectly coupled via the chemical signaling concentration is a very interesting and rich problem. Indeed our preliminary study on the spatiotemporal dynamics of this system reveals that the oscillatory wave can be excited in the system that could serve as a prototype model for the study of intercellular signaling dynamics.

Furthermore, the idea of quorum sensing can be generalized and applied to investigate a mixture of excitable and nonexcitable cells to understand the emergence of spontaneous synchronized oscillation as the relative populations of the cells are changed. For example, mixed cultures of neurons and glial cells can be studied and the effects of interaction between neurons and glial cells [17] on the dynamical behavior might be interpreted in terms of quorum sensing in the broad sense. Also some interesting physiological phenomena in cardiac myocytes and fibroblasts mixture [15,18], such as the dependence of conduction velocity and variability of beating rate on the percentage of fibroblasts [19], can be studied and modeled by the FHN-type QS model in terms of myocyte-fibroblast coupling, which is closely related to experiments. In particular, different ratios of fibroblast occupation to myocytes will induce different beating frequencies and the associated variabilities [20] can be modeled by a two-dimensional coupled network FHN-type QS system.

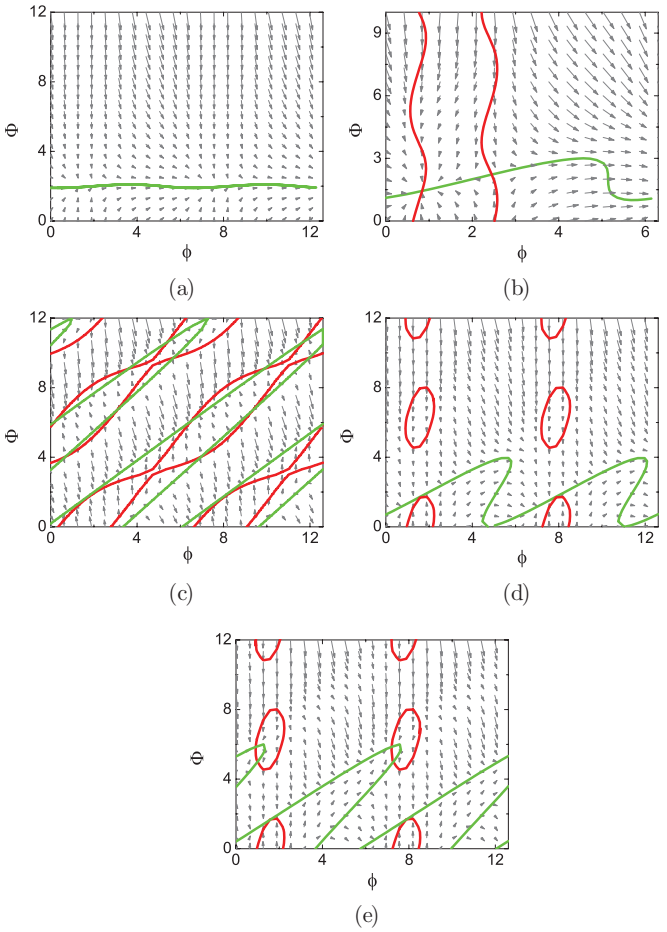

FIG. 12. (Color online) Nullclines and flow in the ϕ-Φ phase plane for various parameter regimes corresponding to Fig. 1. $\dot{\Phi} = 0$ nullclines are green and $\dot{\phi} = 0$ nullclines are red. (a) $b + g < 1$: there is no $\dot{\phi} = 0$ nullcline since it can never be satisfied and the system always remains oscillatory; $b = 0.95$, $g = 0.02$. (b) $b > g + 1$: $\dot{\phi} = 0$ nullclines are vertical nonintersecting curves; $b = 1.5$, $g = 0.2$. (c) $b < g - 1$: $\dot{\phi} = 0$ nullclines are diagonal nonintersecting curves; $b = 0.95$, $g = 2.0$. The $b + g > 1$ and $b^2 + 2bg\cos\Phi_0 + g^2 < 1$ regime: $b = 1.02$, $g = 0.2$. $\dot{\phi} = 0$ nullclines are closed loops, for (d) $\Gamma = 10$ (oscillatory), and (e) $\Gamma = 20$ (quiescent).

ACKNOWLEDGMENTS

This work was supported by the National Science Council of Taiwan under Grant No. 98-2112-M-008-023-MY3, and by NCTS of Taiwan. P.Y.L. thanks the Mathematics Department of UBC for the hospitality in which a major part of this work was accomplished.

APPENDIX: NULLCLINES, PHASE PORTRAITS OF THE QS PHASE MODEL

The nullclines for the system is shown in Fig. 12 showing that the $\dot{\phi} = 0$ nullcline is periodic in both ϕ and Φ directions while the $\dot{\Phi} = 0$ nullcline is periodic only in the ϕ direction. The $\dot{\Phi} = 0$ nullcline is a periodic wavy curve that runs horizontally in the ϕ direction. Larger values of Γ will result in more wavy and tilted crests. Different values Φ_0 merely shift the Φ nullcline up and down. Note that in the $b + g < 1$ region [Fig. 12(a)], $\dot{\phi} = 0$ can never be satisfied and its nullclines

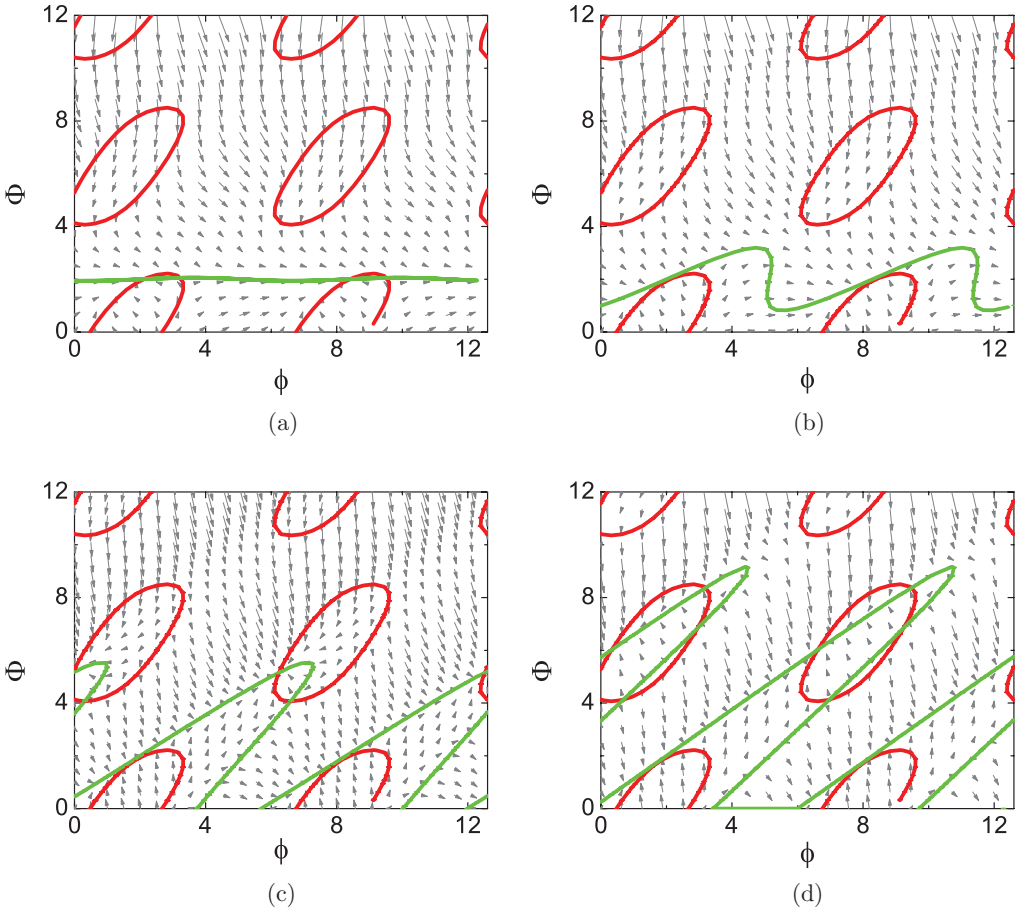

FIG. 13. (Color online) Nullclines and flow in the ϕ-Φ phase plane for the $b^2 + 2bg\cos\Phi_0 + g^2 > 1$ regime. $\dot{\Phi} = 0$ nullclines are green and $\dot{\phi} = 0$ nullclines are red closed loops. $b = 1.02$, $g = 1.2$ for (a) $\Gamma = 0.05$, (b) $\Gamma = 1$, (c) $\Gamma = 3$, and (d) $\Gamma = 6$.

disappear and hence the systems remain always oscillatory. The topology of the $\dot{\phi} = 0$ nullclines are qualitatively different in different parameter regimes in the b-g plane as depicted in Fig. 1. It can be shown [21] that the $\dot{\phi} = 0$ nullcline is a closed loop in the unshaded region (including the QS regime) with the center of each loop fixed periodically in the phase plane and the loop size controlled by the values of b and g. The loop deforms and becomes two nonintersecting curves in the $|b - g| > 1$ regions [see Figs. 12(b) and 12(c)], and the nullcline disappears in the $b + g < 1$ regime. In the regime bounded by $b + g > 1$ and $b^2 + 2bg\cos\Phi_0 + g^2 < 1$, the nullclines do not intersect resulting in oscillatory behavior for low Γ [Fig. 12(d)], but as Γ increases to larger values, the $\dot{\Phi} = 0$ nullcline becomes strongly wavy, intersecting the $\dot{\phi} = 0$ loops, and the system becomes quiescent [Fig. 12(e)].

Figure 12 shows the nullclines and the flow fields in the phase plane corresponding to different parameter regimes in Fig. 1. It is also worth noticing that $\dot{\phi} > 0$ outside the loop and $\dot{\phi} < 0$ inside the loop. Using arguments involving flow fields in the phase plane, one can show that whenever there are intersections of the two nullclines there is always only one stable fixed point and the rest are saddles. This can also be verified from the flow fields of the phase portraits in Fig. 12. When there is no intersection of the nullclines, ϕ increases for all time with trajectories staying close to the Φ nullcline characterizing the oscillatory behavior.

The nullclines and phase portraits for the QS parameter regime are shown in Fig. 13. For low values of Γ [Fig. 13(a)], the $\dot{\Phi} = 0$ nullcline is only slightly wavy and intersects each $\dot{\phi} = 0$ loop at two points resulting in a quiescent state. As Γ increases above some critical Γ_c [Fig. 13(b)], the $\dot{\Phi} = 0$ nullcline becomes so wavy and the crests are so tilted that it no longer intersects with the loops, giving rise to an oscillatory state. Further increasing Γ to another threshold Γ_u makes a huge wavy curve in $\dot{\Phi} = 0$ resulting in new intersections with another periodic loop, thus making the system re-enter quiescence [Fig. 13(c)]. In some scenarios, as depicted in Fig. 13(d), the $\dot{\phi} = 0$ loop intersects the $\dot{\Phi} = 0$ nullcline at four locations, but only one (leftmost) fixed point is stable; the other three fixed points are saddles.

[1] A. R. Gingle, J. Cell. Sci. **20**, 1 (1976).
[2] M. H. Cohen, J. Theor. Biol. **31**, 101 (1971).
[3] A. A. Polezhaev *et al.*, IEE Proc.-Syst. Biol. **1522**, 75 (2005).
[4] B. M Ahmer, Mol. Microbiol. **52**, 933 (2004).
[5] S. De Monte *et al.*, Proc. Natl. Acad. Sci. **104**, 18381 (2007).
[6] T. Greor *et al.*, Science **328**, 1021 (2010).

[7] M. B. Miller and B. L. Bassler, Annu. Rev. Microbiol. **55**, 165 (2001).
[8] S. C. Pratt, Behav. Ecol. **16**, 488 (2005).
[9] T. D. Seeley, P. K. Visscher, and K. M. Passino, Am. Sci. **94**, 220 (2006).
[10] A. F. Taylor *et al*., Science **323**, 614 (2009).
[11] Y. Kuramoto, *Chemical Oscillations, Waves and Turbulence* (Springer-Verlag, Berlin, 1984).
[12] A. Pikovsky, M. Rosenblum, and J. Kurths, *Synchronization: A Universal Concept in Nonlinear Sciences* (Cambridge University Press, Cambridge, England, 2003).
[13] R. FitzHugh, Biophys. J. **1**, 445 (1961); J. Nagumo, S. Arimoto, and S. Yoshizawa, Proc IRE **50**, 2061 (1962).
[14] XPPAUT, http://www.math.pitt.edu/~bard/xpp/xpp.html.
[15] W. Y. Chiang, P. Y. Lai, and C. K. Chan, Phys. Rev. Lett. **106**, 254102 (2011).
[16] B. A. Hense, C. Kuttler, J. Muller, M. Rothballer, A. Hartmann, and J. U. Kreft, Nat. Rev. Microbiol. **5**, 230 (2007).
[17] X. Zhan, P. Y. Lai, and C. K. Chan, Phys. Rev. E **84**, 011907 (2011).
[18] W. Chen *et al*., Europhys. Lett. **86**, 18001 (2009).
[19] J. P. Fahrenbach *et al*., J. Physiol. **583**, 565 (2007).
[20] W. Y. Chiang, P. Y. Lai, and C. K. Chan (unpublished).
[21] Y. X. Li and P. Y. Lai (unpublished).